

Lab on a Chip

Accepted Manuscript



This is an *Accepted Manuscript*, which has been through the Royal Society of Chemistry peer review process and has been accepted for publication.

Accepted Manuscripts are published online shortly after acceptance, before technical editing, formatting and proof reading. Using this free service, authors can make their results available to the community, in citable form, before we publish the edited article. We will replace this *Accepted Manuscript* with the edited and formatted *Advance Article* as soon as it is available.

You can find more information about *Accepted Manuscripts* in the [Information for Authors](#).

Please note that technical editing may introduce minor changes to the text and/or graphics, which may alter content. The journal's standard [Terms & Conditions](#) and the [Ethical guidelines](#) still apply. In no event shall the Royal Society of Chemistry be held responsible for any errors or omissions in this *Accepted Manuscript* or any consequences arising from the use of any information it contains.



Lab on a Chip

COMMUNICATION

Microfluidic vascularized bone tissue model with hydroxyapatite-incorporated extracellular matrix

Norhana Jusoh^{a,b,+}, Soojung Oh^{a,c,+}, Sudong Kim^a, Jangho Kim^{d,*} and Noo Li Jeon^{a,c,*}

Received 00th January 20xx,
Accepted 00th January 20xx

DOI: 10.1039/x0xx00000x

www.rsc.org/

Current *in vitro* systems mimicking bone tissues fail to fully integrate the three-dimensional (3D) microvasculature and bone tissue microenvironments, decreasing similarity to *in vivo* conditions. Here, we propose 3D microvascular networks in hydroxyapatite (HA)-incorporated extracellular matrix (ECM) for designing and manipulating a vascularized bone tissue model in a microfluidic device. Incorporation of HAs of various concentrations resulted in ECM with varying mechanical properties. Sprouting angiogenesis was affected by mechanically modulated HA-extracellular matrix interactions generating a model of vascularized bone microenvironment. Using this platform, we observed that hydroxyapatite enhanced angiogenic processes such as sprout length, sprouting speed, sprout number, and lumen diameter. This new platform integrates fibrin ECM with the synthetic bone mineral HA to provide *in vivo* like microenvironments for bone vessel sprouting.

Recently, microfluidic devices have been engineered to mimic tissues and organs to model physiological cellular microenvironment. Further development of these microfluidic models have begun to generate *in vitro* disease (i.e. cancer) states for drug screening and understanding of biological mechanism. Organs on chip show great potential as alternatives for replacing animal testing for biomedical, pharmaceutical, and toxicological applications¹. Consequently, microvascular systems have been proposed as efficient three-dimensional (3D) *in vitro* models for studying complex biological phenomena in living systems^{1,2}.

Specifically for vascularized bone tissue models, microfluidic

devices have been developed to investigate breast cancer metastasis to the bone and cancer extravasation using an osteo-cell condition microenvironment². The *in vitro* platforms of vascularized bone models have also been engineered to evaluate angiogenic potential³ and for coupling with osteogenesis⁴. For breast cancer bone metastasis, *in vitro* mineralized tumors were developed solely with cancer cells and were able to induce secondary tumor formation⁵. Bone angiogenesis has important roles in endochondral bone formation and repair⁶. However, these *in vitro* methods, either conventional or microfluidic platforms, were not able to mimic the *in vivo* bone angiogenesis that is involved in vessel sprouting within the mineralized bone matrix. Note that an ideal platform for engineering bone tissue should have suitable 3D structures with interconnected pores to facilitate cellular activities while maintaining sufficient mechanical strength to support cell adhesion, proliferation, and differentiation⁷⁻¹².

Here we report a new platforms incorporating hydroxyapatite (HA) into the microfluidic chip as mineralized bone tissue models for mimicking real bone angiogenesis. To this end, fibrin, as a model extracellular matrix (ECM), was combined with HA nanocrystals in order to mimic a real bone tissue matrix with highly porous and interconnected structures of HA-fibrin scaffolds to induce vessel sprouting (Fig. 1). Using this platform, we observed that hydroxyapatite enhanced angiogenic processes such as sprout length, sprouting speed, sprout number, and lumen size.

The microfluidic device consists of four parallel channels separated by 100 μm gaps using microposts, and this also facilitated paracrine communication between endothelial cells (ECs) and stromal cells during vessel formation, as shown in Fig. 1(a-c). Note that we designed channels with 100 μm micropost gap to prevent leakage and capture the hydrogels in the microfluidic device⁸. Lung fibroblasts (LFs) were selected as stromal cells due to their capability to secrete pro-angiogenic growth factors and ECM proteins that enhance human umbilical vein endothelial cell (HUVEC) morphogenesis⁹. The microfluidics also enable separate and simultaneous tuning of biomechanical and biochemical simulation, resulting in discrete changes in matrix density, growth factor concentration, growth factor gradient steepness, which are

^aSchool of Mechanical and Aerospace Engineering, Seoul National University, Seoul, 151-744, South Korea. E-mail: njeon@snu.ac.kr; Tel: +82-2-880-7111

^bFaculty of Biosciences and Medical Engineering, Universiti Teknologi Malaysia, Skudai, Johor, 80990, Malaysia.

^cInstitute of Advanced Machinery and Design (SNU-IAMD), Seoul National University, Seoul, 151-744, South Korea.

^dDepartment of Rural and Biosystems Engineering, Chonnam National University, Gwangju, 500-757, South Korea. Email: rain2000@jnu.ac.kr; Tel: +82-62-530-5181

[†]Electronic Supplementary Information (ESI) available: [Additional results]. See DOI: 10.1039/x0xx00000x

*Corresponding authors

[‡]These authors contributed equally to the work

important during the stages of early sprout initiation, sprout elongation, sprout navigation, and lumen formation¹³.

Containing HA nanoparticles in the fibrin ECM, these platforms more closely resemble *in vivo* bone tissue, which is mainly composed of stiff ECM and calcium phosphate minerals that contribute to the hardness and rigidity of bone. Fig. 1(d) shows various structures consisting of pure fibrin (0% HA) and fibrin with 0.05% HA, 0.10% HA, 0.30% HA, 0.4% HA and 0.50% HA. The images show that the HA particles distributed homogeneously within the fibrin hydrogel and the HA particles can be readily seen with increasing HA concentrations in the microfluidic chip (Fig. 1, S1, S2, and Table S1). We have confirmed that the fibrin and HA polymerization was limited up to 0.4% HA. With 0.5% HA and above, the mixture of fibrin and HA could not polymerize in the microfluidic channel to form hydrogel-like structures, as shown in Fig. 1(d). In addition, to confirm the distribution of HA within the fibrin in the microfluidic channel, we treated the fibrin-HA hydrogel with the hydrophilic dye Trypan Blue^{14,15} (Fig. 1(e)). Moreover, Trypan Blue that selectively stained the ceramics was used as a nonspecific indicator of adsorption potential of HA¹⁵. As shown in Fig. 1(e), Trypan Blue does not adsorb into fibrin hydrogel, but incorporation of HA induces greater dye adsorption to the hydrogel. Thus, incorporation of HA alters protein adsorption¹⁵.

To confirm the effects of HA on blood vessel formation, we conducted angiogenesis experiments using various HA concentrations. Fig. 2(a) shows examples of bright field images, while Fig 2(d) shows confocal images of angiogenic vascular networks that were established with 0.0% HA and 0.2% HA. Immunostaining indicates the expression of the EC marker CD31 was concentrated at junctions between adjacent cells. Fig. 2(b) shows the quantification of angiogenic sprout growth for various HA concentrations.

With the addition of HA into the fibrin hydrogel, the average sprout length increased from 593 μm to 694 μm for 0.0% and 0.2% HA, respectively. On the other hand, 0.3% and 0.4% HA slightly decreased sprout length, which were 635 μm and 585 μm , respectively. Thus, these results suggest that the sprout length for 0.0% and 0.4% HA were comparable. Fig. 2(b) shows the average speed of vessel sprouting from day 3 to day 4. Vessel sprouting for 0.2% HA exhibited the fastest speed at 6 $\mu\text{m}/\text{h}$, followed by 0.4% HA and 0.1% HA with 3 $\mu\text{m}/\text{h}$ for both conditions. For 0.0% HA and 0.30% HA, the sprouting speed was 2 $\mu\text{m}/\text{h}$ and 1 $\mu\text{m}/\text{h}$, respectively. We have learned that the fibrin gels started to induce fiber aggregation when HA concentration was increased (i.e., > 0.4% HA), resulting in non-uniform hydrogel formation. Therefore, the endothelial cells might penetrate deep into the coarse structures of hydrogel, which might enhance the angiogenesis speed in the 0.4% HA-fibrin gels than 0.3% HA-fibrin gels in the microfluidic devices. Incubation of ECs with crystallized HA favored cell adhesion, spreading, and proliferation, inducing an activation of cytoskeletal architecture without any cytotoxic effect. HA nanocrystals exhibit high biocompatibility for microvascular endothelium, maintaining biochemical markers of healthy endothelium and expressing markers of functional endothelium that might contribute to angiogenesis.

We also determined the effect HA on lumen formation for 0.0% HA and 0.2% HA, as shown in Fig. 2(d) and Fig. 2(e). The average

lumen area for 0.2% HA (5963 μm^2) was greater than 0.0 % HA (4044 μm^2). Fig. 2(e) shows that the number of sprouts at day 4 were 19 and 26 for 0.0 % HA and 0.2% HA, respectively. This result suggests that the number of sprouts was increased by the addition of HA into the fibrin. Besides chemical cues such as growth factors, mechanical cues (matrix stiffening) can also effect blood vessel formation, especially during angiogenesis¹⁶. Hydrogels containing higher HA concentrations were significantly stiffer than pure hydrogel¹¹. Thus, in this work, the fibrin stiffness was tuned by incorporating HA in the hydrogel. ECM stiffness can modulate capillary formation as well as barrier integrity by altering endothelial response to chemical factors¹⁶. The difference values in Fig. 2(e) indicate that lumen formation is more favorable in an HA environment, which is stiffer than pure fibrin. These results are supported by the previous findings that more stable and larger lumens are formed with increasing gel stiffness observed in 3D rigid gels^{13,17}. Matrix stiffness also influences EC elongation and sprouting in 3D environments, resulting in enhanced sprouting and outgrowth¹⁸. In addition, thicker and deeper vessel networks were formed with the increasing stiffness¹⁷. Thus, the HA-fibrin stiffness affects the number of sprouting vessels.

Fig. 3 shows a schematic depiction of a proposed model for the effects of HA particles on bone angiogenesis that might be occurring in this study. One of the important factors in developing bone-mimicking scaffolding material is the ability to favor ECs, which typically occurs via growth factors such as vascular endothelial growth factors (VEGFs) that have been reported as critical chemotactic factors for vasculogenesis and angiogenesis. VEGFs are also involved in osteoblast and osteoclast differentiation and appear to enhance bone growth and repair *in vivo*¹⁹. VEGFs are able to adsorb into HA nanocrystal surfaces and are able to accelerate angiogenesis^{19,20}. There is a strong electrostatic attraction between VEGFs and HAs during the adsorption of VEGFs onto micro- or nanoscale HA surfaces²⁰. Therefore, HA has been widely used as a VEGF delivery system. Compared to high concentrations of VEGF release, sustained release of VEGF increased the efficacy of VEGF delivery with prolonged bioavailability of low concentrations of VEGF, which is more beneficial for bone regeneration²¹. Continuous delivery of low concentrations of VEGFs from calcium phosphate ceramics might increase the efficacy of the administration of VEGFs²¹. Moreover, mesoporous HA (MHA), with various pore sizes, which were infused with VEGFs can gradually release VEGF and enhance revascularization²⁰. Gradual release and accumulation of VEGF could promote the proliferation of HUVECs and lead to rapid vascularization after implantation²⁰. On the other hand, increasing HA concentration will increase growth factor adsorption and will enhance sprout formation only up to a certain level. After this optimum level, sprout formation will be reduced with excess HA. High local concentrations of VEGF result in the formation of malformed and non-functional vessels due to changes in angioblast behavior in normally avascular areas²². High local concentrations of VEGF also cause the loss of individual vessel identity due to alterations in vessel lumen formation and vessel patterning, resulting from the unregulated and excessive fusion of vessels²². Furthermore, matrix metalloproteinases (MMPs) expression increases with increasing stiffness, resulting in decreasing vessel

density²³. MMPs regulate the vascular structure by degrading elastic fibers and inhibiting angiogenesis by generating angiostatin, which results in the reduction of microvascular density. Taken together, HA particles might play an important role in 3D bone angiogenesis during the bone development process.

Conclusions

Bone is a highly vascularized tissue but lack a good *in vitro* model that reflect complex chemical (i.e. growth factor trapping) and mechanical (i.e. stiffness) microenvironment. We have successfully constructed bone angiogenesis model in a microfluidic device to overcome the limitations of current *in vitro* models. This new platform integrates fibrin ECM with the synthetic bone mineral HA to provide *in vivo* like microenvironments for bone vessel sprouting. Formation of angiogenic networks was observed as function of various HA concentrations. This bone angiogenesis platform is relevant for various applications, including drug screening and as a bone disease (i.e. metastasis to bone) model. We conclude that our HA-incorporated 3D microvascular networks offer a new approach for the investigation of complex biological phenomena as well as for analysis of drug responses and toxicities in bone tissues.

Acknowledgements

This work was supported by the Brain Korea 21 Plus Project in 2015 (F14SN02D1310), the National Research Foundation funded by the Ministry of Education (NRF-2015R1A2A1A09005662), the Ministry of Food and Drug Safety in 2015 (15182MFDS455), the Korean Health Technology R&D Project, Ministry of Health & Welfare, Republic of Korea (Grant No. H14C14000), and a grant (714002-7) from the Agricultural Robotics and Automation Research Center through Agriculture, Food and Rural Affairs Research Center Support Program, Ministry of Agriculture, Food and Rural Affairs.

Notes and references

- 1 D. Huh, Y. Torisawa, G. A. Hamilton, H.J Kim, and D. E. Ingber, *Lab Chip*, 2012, **12**, 2156.
- 2 S. Bersini, J. S. Jeon, G. Dubini, C. Arrigoni, S. Chung, J. L. Charest, M. Moretti M, R.D Kamm, *Biomaterials*, 2014, **35**(8), 2454.
- 3 E. Cenni E, F. Perut F, N. Baldini, *Acta Pharmacologica Sinica*, 2011, **32**, 21.
- 4 C. Correia, W. L Grayson, M. Park, D. Hutton, B. Zhou, X. E. Guo, L. Niklason, R. A. Sousa, R. L. Reis, G. Vunjak-Novakovic, *Plos One*, 2011, **6**(12), e28352.
- 5 S. P. Pathi, C. Kowalczewski, R. Tadipatri and C. Fischbach, *PLoS ONE*, 2010, 5(1).
- 6 (a) R. A. Carano and E. H. Filvaroff, *Drug Discov Today*, 2003, **8**(21), 980; (b) M Kanczle and R. O. C Oreffo, *European Cells and Materials*, 2008, **15**, 100.
- 7 Z. Xia, M. M. Villa and M. Wei, *Journal of Materials Chemistry B*, 2014, **2**, 1998
- 8 (a)S. Kim, H. Lee, M. Chung and N. L. Jeon, *Lab Chip*, 2013, **13**, 1489; (b) J. A. Whisler, M. B. Chen and Kamm, R. D., *Tissue Engineering Part C Methods*, 2013, **20**(7), 543.
- 9 T. Osathanon, M. L. Linnes, R. M. Rajachar, B. D. Ratner, M. J. Somerman and C. M. Giachelli, *Biomaterials*, 2008, **29**(30), 4091.
- 10 (a)S. Pezzatini, R. Solito, L. Morbidelli, S. Lamponi, E. Boanini, A. Bigi, M. Ziche, *J Biomed Mater Res A*, 2006, **76**(3):656-663; (b) M. R. Appleford, S. Oh, N. Oh, J. L Ong, *Journal of Biomedical Materials Research Part A*, 2009, **9**(4), 1019.
- 11 R. R. Rao, J. Ceccarelli, M. L Vigen, M. Gudur, R. Singh, C. Y. Deng, A. J. Putnam, J. P. Stegemann, *Acta Biomaterialia*, 2014, **10**, 3091.
- 12 E. Lammert and J. Axnick, *Cold Spring Harb Perspectives in Medicine*, 2012, **2**, a006619
- 13 A. Shamloo and S. C. Heilshorn, *Lab Chip*, 2010, **10**, 3061
- 14 J. He, D. C. Genetos and J. K. Leach, *Tissue Engineering: Part A*, 2010, **16** (1).
- 15 S. Kim, M. S. Park, O Jeon, C. Y. Choi, B. Kim, *Biomaterials*, 2006, **27**, 1399–1409.
- 16 D. J. LaValley and C. A. Reinhart-King, *Advances in Regenerative Biology*, 2014, **1**, 25247.
- 17 N. Yamamura, R. Sudo, M. Ikeda and K. Tanishita, *Tissue Eng*, 2007, **13**, 1443.
- 18 B. N. Mason, A. Starchenko, R. M. Williams, L. J. Bonassar, C. A Reinhart-King, 2013, *Acta Biomater*, 2013, **9**, 4635.
- 19 V. Midy, E. Hollande, C. Rey, J. M. Dard and T. Plouet *Journal of Materials Science: Materials in Medicine*, 2001, **12**, 293.
- 20 (a) C. K. Poh, S. Ng, T. Y. Lim, H. C. Tan, J. Loo, W. Wang, *J Biomed Mater Res Part A*, 2012, **100A**, 3143; (b) Y. Chen, J. Wang, X. Zhu, Y. Fan and X. Zhang, *Journal of Biomaterials and Tissue Engineering*, 2014, **4** (2), 155.
- 21 E. Wernike, M. O. Montjovent, Y. Liu, D. Wismeijer, E. B Hunziker, K. A. Siebenrock, W. Hofstetter and F. M. Klenke *European Cells and Materials*, 2010, **19**, 30.
- 22 C. J. Drake and C. D. Little, *Proc. Natl. Acad. Sci. USA*, 1995, **92**, 7657.
- 23 A. W. Y. Chung, H. H. C. Yang, M. K. Sigrist, G. Brin, E. Chum, W. A. Gourlay and A. Levin, *Cardiovasc Res*, 2009, **84**, 49

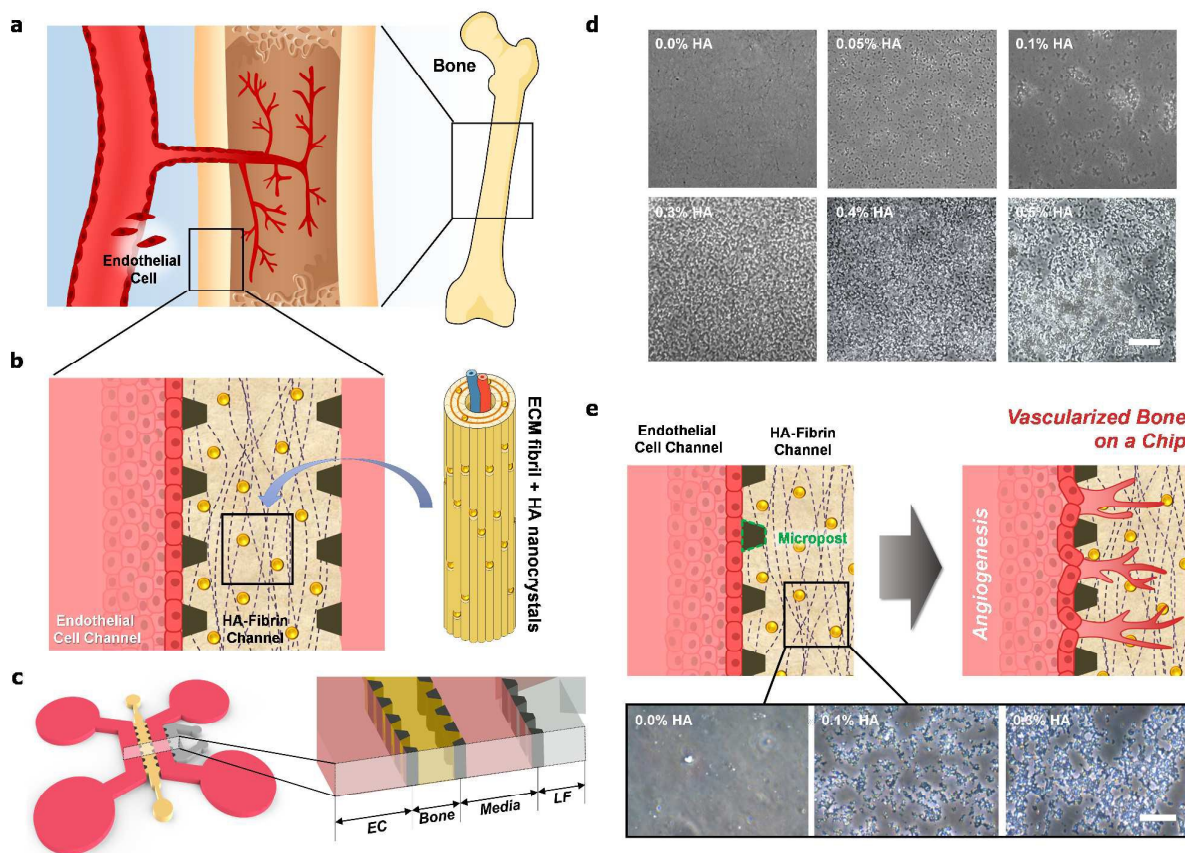


Fig. 1 Rational design and fabrication of microfluidic vascularized bone tissue model with hydroxyapatite-incorporated extracellular matrix (ECM). (a) Angiogenesis during bone development. (b) HA nanocrystals and fibrin ECM encapsulating the blood vessel. (c) Schematic of the microfluidic chip. (d) Cell seeding configuration for angiogenesis with images of fibrin incorporated with 0.00%, 0.05%, 0.10%, 0.30, 0.40, and 0.50%. With 0.5% HA and above, the mixture of fibrin and HA could not polymerize in the microfluidic channel to form hydrogel-like structures. Scale bar: 50 μm . (e) Fibrin and HA polymerization (0.0%, 0.1% and 0.3% HA) after treatment with Trypan Blue. Scale bar: 25 μm .

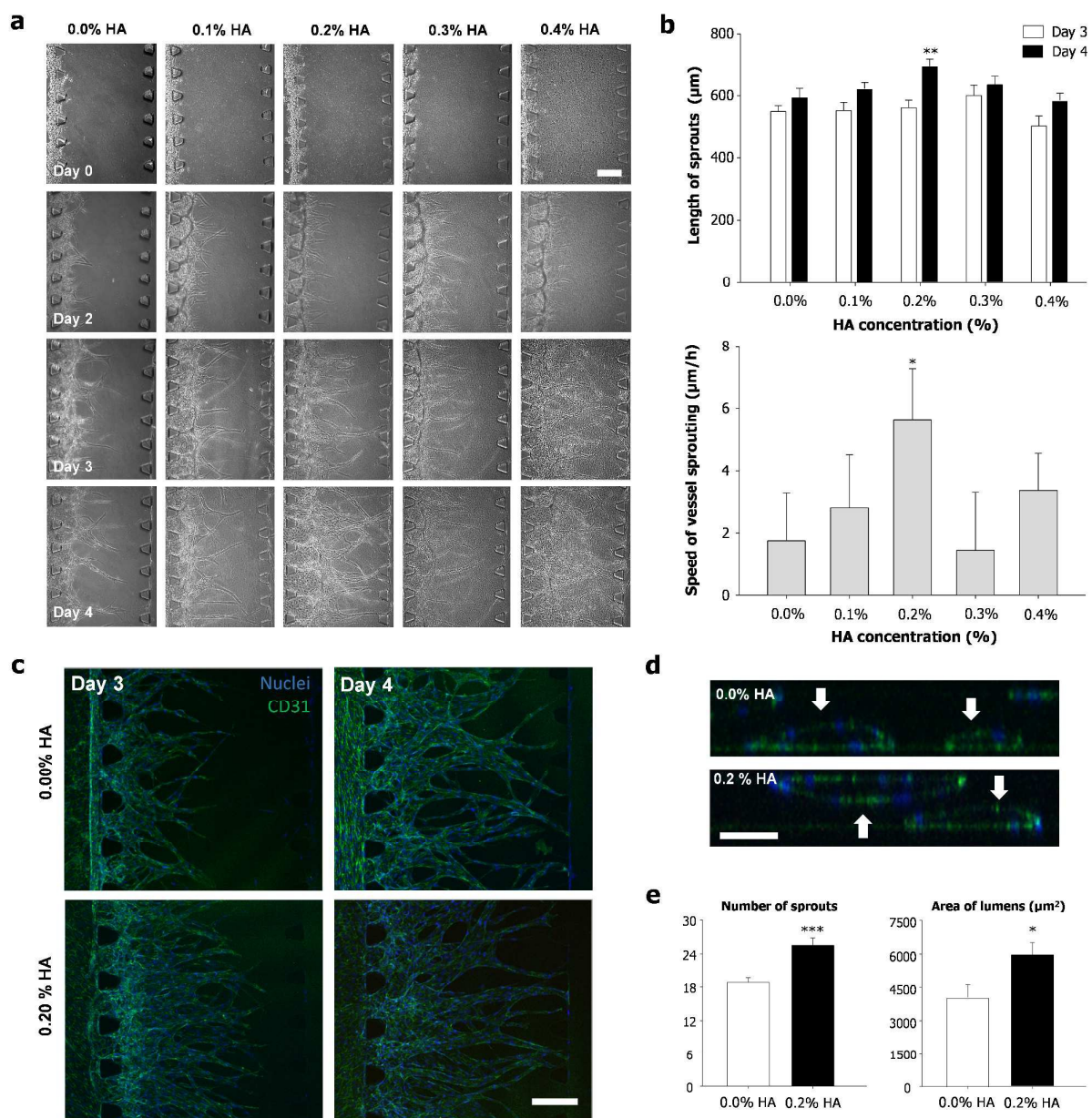


Fig 2 Enhanced angiogenic processes in microfluidic devices with hydroxyapatite-incorporated extracellular matrix. (a) Bright field images of angiogenic vascular networks established. (b) Quantification of angiogenic sprout growth ($n=20$, $P < 0.01$) and average speed of vessel sprouting ($n=20$, $P < 0.05$). (c) Confocal images of vascular networks established by angiogenesis that were stained for CD31 (green) and for nuclei (blue). (d) Cross-sectional images of hollow lumens enclosed by HUVECs. (e) Quantification of sprout number at day 4 ($n=20$, $P < 0.001$) and area of lumens at day 4 ($n=20$, $P < 0.05$). Scale bar: 200 μm . Error bars represent SEM.

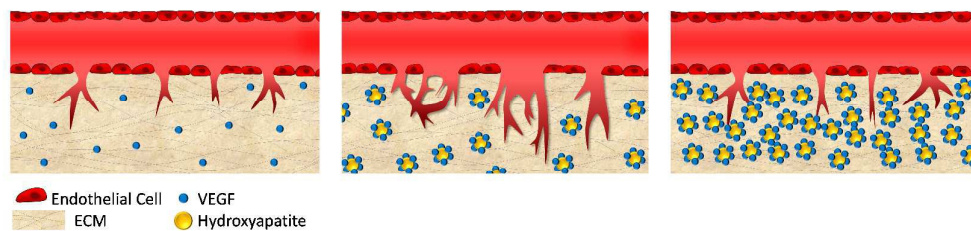


Fig. 3 Schematic depiction of a proposed model for the effects of HA particles on bone angiogenesis. The HA particles might adsorb growth factors (e.g., VEGFs), which might accelerate angiogenesis^{19,20}. On the other hand, excessive HA particles might not allow enough space for enhancing angiogenesis